Accepted Manuscript

Pulse-Transient Adapted C-Symmetry Pulse Sequences

Johannes Weber, Marten Seemann, Jörn Schmedt auf der Günne[*],

Ludwig-Maximilians-Universität, Department Chemie,

Butenandtstr. 5-13 (Haus D), 81377 München, Germany

February 17, 2012

[*]corresponding author; Email Address: gunnej@cup.uni-muenchen.de

Abstract

In solid-state NMR, pulse sequences make often use of pulses which are short compared to the recovery time of the probe head. Especially, rotorsynchronized dipolar recoupling experiments under magic-angle-spinning conditions can profit from the use of very high pulse amplitudes which in turn will reduce the length of the individual pulses. In this contribution we show that C-symmetry based pulse sequences used for double-quantum filtering experiments can strongly be influenced by pulse transients. We analyze the origin of pulse transients and show that the quadrature component can be minimized by cable-length variation which causes a mutual cancellation of probe-external and internal contributions. We implement and test a model to investigate the influence of pulse-transients by numerically exact calculations of the spin-density matrix allowing for composite pulses consisting of slices which are short compared to the circuit recovery time-constant. Moreover we introduce a phase-tuned C-element, which can be applied to γ-encoded experiments from the C-symmetry class, to reconstitute an almost ideal performance of the sequence. We have validated the modified transient-adapted pulse sequences theoretically on the basis of numerically exact calculations of the spin-dynamics. While comparably easy to apply the scheme proved also robust in practical application to ^{15}N, ^{13}C and ^{31}P double-quantum filtered experiments and leads to a significantly increased conversion efficiency.

keywords: NMR, solid-state, pulse transients, C-sequences

1 Introduction

Pulse transients occur in any real NMR spectrometer and refer to the transient difference between the intended pulse-shape and the pulse-shape which finally manipulates the nuclear spin-states in the sample coil of the NMR probe head. For a simple series RLC circuit pulse transients become more pronounced the longer the rise-/recovery-times of the probe circuit τ_R, which is given by [1, 2]

$$\tau_R = \frac{2}{\Delta\omega} = \frac{2Q}{\omega_0} \tag{1}$$

where $\Delta\omega$ is its band-width, Q the quality factor [2] of the probe[1] and $\omega_0 = \sqrt{\frac{1}{LC}}$ its natural frequency. Pulse transients can make the real pulse deviate from the intended pulse-shape both in pulse amplitude and pulse phase, which generally leads to a degraded performance of pulse sequences.

The NMR community has long been aware of pulse transients. There are special probes for experiments, like the CRAMPS experiment [3], which are known to be sensitive to pulse transients. These probes are designed to have a lower quality factor Q ($Q = \frac{\omega_0}{\Delta\omega}$) in order to shorten the rise-time τ_R of the electronic circuits. However this is bought with a decreased signal-to-noise ratio which is correlated to the quality factor Q [2, 4]. Thus most commercial probes follow the design principle of a high Q value. Pulse transients are known to potentially influence pulse sequences with long cyclic pulse trains [1, 5] and need to be taken into account if the individual piece-wise constant slices of a multi-pulse sequence are short compared to τ_R. Clearly, modern sequences designed through optimal control [6], double-frequency sweeps [7] or different windowless symmetry-based pulse sequences [8] are influenced much stronger by pulse

---

[1]The NMR probes heads here are considered to be series RLC circuits.

transients than the simple spin-echo experiment or short windowed pulse-sequences like BABA [9] because of fast amplitude and phase modulations being used. The influence of pulse transients has been investigated for different pulse sequences in detail. For the CRAMPS-type experiments it was shown that transients can be reduced [1, 3, 5, 10, 11] to such an extent that they are no longer the line-width limiting factor. For symmetry based experiments [8, 12] the influence of pulse-transients [10, 13, 14] seems to depend on the actual conditions of the experiment. Here we want to investigate the influence of pulse transients on specific C-symmetry based pulse sequences namely double-quantum filtered pulse sequences for which pulse transients can have a strong influence [14, 15].

How can the influence of pulse transients on pulse sequences be modeled in the computer? Any discontinuity in pulse phase, amplitude and frequency will cause pulse transients. For a probe solely consisting of linear passive electronic elements like capacitors, coils and resistors the time dependence can be predicted using linear time-invariant system (LTI) theory [16], which neglects however important non-linear elements like power amplifiers and diodes of the duplexer present in the signal pathway. Pulse sequences with a constant pulse frequency which show several discontinuities in pulse phase or/and pulse amplitude can then simply be described by a superposition of the system response in the time domain caused by the individual discontinuities. Alternatively, an elegant solution is to apply the transient behavior to the intended pulse-shape by switching from a time based description to another domain which is generated by the Laplace transform [16, 17]. Here we stick to a description in the time domain. Several functions have been described which are supposed to give the response of a simple system of a NMR probehead to a single pulse discontinuity [1, 5, 13, 18]. These functions describe the response of a real system with a limited number of parameters.

Analytical functions to describe the response function to a single discontinuity, split

4

the pulse-transient into different terms/contributions, which can be given a physical meaning for simple networks. Components which have the same pulse phase as the steady-state current to which they relate are called *in-phase* contributions [1, 5, 18], while components which are off in pulse-phase are called *quadrature* contributions [1, 5, 18]. Moreover there are contributions related to the "real" turn-off or turn-on pulse-phase, i.e. not the pulse-phase which is defined relative to the receiver phase. The latter contribution may be neglected for our probe heads ($Q > 50$) however, because it scales with $\frac{1}{4Q}$ [5, 18].

Experimentally, the operator has several options at hand to influence pulse transients. It was soon realized that a number of methods exist to suppress the quadrature contribution, for example by tuning the system [19] with special tune-up sequences [20–22], by damping or removing reflections in the transmission lines to the probe head with the help of circulators/isolators [3], high-power attenuators or through varying the cable length[2]. The in-phase contribution may be influenced through the rise-time, i. e. the bandwidth, of the probe head. This may be achieved passively by lowering the Q-value simply by adding a resistor to the series RLC circuit or more efficiently by switching between a high Q value during the acquisition of the free induction decay and a low Q value during the pulse [23–25]. Moreover active-feedback circuits [17] have been shown to almost completely cancel the effect of pulse transients for both the in-phase and quadrature component.

The purpose of this contribution is to study the influence of pulse transients on double-quantum filtered pulse-sequences, to implement a simple scheme to model the effect of transients on multiple-pulse sequences in a computer and to show how the performance for double-quantum filtered experiments (PostC7 [12, 26]) can be reestab-

---

[2]personal communication by Hans Förster (Bruker Biospin)

lished both in theory and experiment without hardware modifications except for cable-length changes. Variations of the cable-lengths will be used to investigate under which circumstances cable-length effects will help to remove the quadrature component to pulse transients.

2 Pulse Transients

2.1 Drive Current and Coil Current

Real pulses on NMR spectrometers differ in many respects from what an ideal radio-frequency pulse is supposed to look like. Transient deviations which are absent for indefinitely long pulses are in short often termed "pulse transients". Pulse transients are expected for any RLC tank circuit and hence for any NMR probehead. Since sample magnetization is affected by the linearly polarized oscillating magnetic field caused by the coil current $I(t)$, the task is essentially to describe the transient deviations of the coil current relative to the current expected from the driving voltage. We will assume that the magnetic field B_{rf} of a pulse is proportional to the coil current.

In the following description we restrict ourselves to multiple pulse sequences which do no involve a change of transmitter frequency ω_{tr}. If necessary, frequency changes can be described in the same framework with the help of phase ramps. Because today's spectrometers work on a digital basis, it is convenient to describe pulses piecewise constant function of phase ϕ, current amplitude A and frequency ω_{tr}, alternatively with the complex current amplitude [27] $\underline{a} = (a_{re} + i\,a_{im})$, where a_{re}, a_{im}, A and ϕ are real.

$$
\begin{aligned}
I(t) &= A\cos(\omega t + \phi) \\
&= Re\left\{A\,e^{i\phi}e^{i\omega_{tr}t}\right\} \qquad\qquad (2) \\
&= Re\left\{(a_{re} + i\,a_{im})e^{i\omega_{tr}t}\right\}
\end{aligned}
$$

The complex notation with the imaginary unit $i^2 = -1$, has the advantage that it is easy to extend to multiple-pulse sequences, because it allows superposition of sinusoidal functions with different phases and amplitudes (see below). The variables a_{re}, a_{im}, A and ϕ can be functions of time, while ω_{tr} is time independent.

In the following part this notation will be used to describe pulse phase and amplitude as a function of time.

2.2 Modeling Pulse Transients

Different models have been proposed in the literature [1, 18, 28] to describe the time dependent response of phase and amplitude after a single junction/discontinuity between two indefinitely long pulses *m* and *n*.

Here we chose a model related to the one by Mehring and Waugh [1, 5], which is based on the LTI analysis of a tank circuit close to its natural oscillation frequency ω_0 [1]. Our simplified version describes transients of a series LCR network with only two parameters: a recovery time constant τ_R as defined in eq. 1 and an "electronic" offset frequency ω_{eoff}, which is the difference between the "free ringing" [5] (or resonance frequency [1]) of the circuit ω_r and the transmitter frequency ω_{tr} of the radio frequency (rf) pulse. This model neglects effects of the turn-off and and turn-on phase as explained

in the introduction. The complex current amplitude $\underline{a}_{total}(t)$ at the time t may be decomposed into *(i)* a *decaying, transient contribution* T_d influenced by the previous segment with phase ϕ_m and amplitude A_m, and *(ii)* a *rising, contribution* $T_r + A_n \exp(i\phi_n)$ of the current segment which consists of a pulse transient T_r with phase ϕ_n and amplitude A_n and the non-transient contribution of the active pulse $A_n \exp(i\phi_n)$, where t refers to a time point after the discontinuity at time t_{mn} in phase and/or amplitude, i.e. $t > t_{mn}$.

$$\underline{a}_{total}(t) = T_d(\phi_m, A_m, t_{mn}, t) + T_r(\phi_n, A_n, t_{mn}, t) + A_n \exp(i\phi_n) \tag{3}$$

The rising and the decaying contribution can be split up into a part in-phase with the pulse-phase and a part out of phase by $\pi/2$ (in quadrature).

$$T_d(\phi_m, A_m, t_{mn}, t) = \underbrace{A_m \exp\left(-\frac{t - t_{mn}}{\tau_R}\right) \cos\left(\{t - t_{mn}\} \omega_{eoff}\right) \exp(i\phi_m) +}_{\text{in phase}} \tag{4}$$
$$\underbrace{A_m \exp\left(-\frac{t - t_{mn}}{\tau_R}\right) \sin\left(\{t - t_{mn}\} \omega_{eoff}\right) \exp\left(i\left\{\phi_m + \frac{\pi}{2}\right\}\right)}_{\text{quadrature}}$$

$$T_r(\phi_n, A_n, t_{mn}, t) = \underbrace{-A_n \exp\left(-\frac{t - t_{mn}}{\tau_R}\right) \cos\left(\{t - t_{mn}\} \omega_{eoff}\right) \exp(i\phi_n) +}_{\text{in phase}} \tag{5}$$
$$\underbrace{-A_n \exp\left(-\frac{t - t_{mn}}{\tau_R}\right) \sin\left(\{t - t_{mn}\} \omega_{eoff}\right) \exp\left(i\left\{\phi_n + \frac{\pi}{2}\right\}\right)}_{\text{quadrature}}$$

Finally we get:

$$\underline{a}_{total}(t) = \exp\left(-\frac{t-t_{mn}}{\tau_R}\right)\exp\left(i\{t-t_{mn}\}\omega_{eoff}\right)[A_m\exp(i\phi_m)-A_n\exp(i\phi_n)]+A_n\exp(i\phi_n)$$

(6)

The observed transient behavior is calculated from the real part of the complex current $\underline{a}_{total}(t)$. As expected transient contributions (first term in eq.(6)) vanish if $\phi_m - \phi_n = 0$ and $A_m - A_n = 0$. The non-zero factor $[A_m\exp(i\phi_m)-A_n\exp(i\phi_n)]$ thus is what drives a pulse-transient into existence.

Note that the original Mehring-Waugh model predicts oscillations in amplitude and phase (Figure 1) [28] which are absent in recently proposed models [13, 18]. Despite the chosen model being closely related to the original Mehring-Waugh model we deliberately use it to describe pulse transients in more complicated networks. The price we pay is that the probe parameters τ_R and ω_{eoff} loose their physical meaning and become empirical parameters to describe a real probe, including filters, amplifier and duplexer.

2.2.1 Pulse Transients in Multiple-Pulse Sequences

The above model described for a single discontinuity will now be extended to the description of transients in a multiple-pulse sequence, that consists of k pulses. Again, a complex current $\underline{a}_{total}(t)$ is to be calculated which describes the amplitude and phase during the last pulse ($t > t_{k(k+1)}$). The transient is then expected to be a simple superposition of transients caused by any discontinuity in phase and/or amplitude prior to the time t for which the complex current is to be calculated, i.e.:

9

$$a_{total}(t) = A_k \exp(i\phi_k) + \sum_{p=1}^{k-1} \left[T_d(\phi_p, A_p, t_{p(p+1)}, t) + T_r(\phi_{p+1}, A_{p+1}, t_{p(p+1)}, t) \right] \quad (7)$$

2.3   Validation of the transient model

How well is the simplified Mehring-Waugh model able to describe the pulse transients in a real spectrometer? Is it possible to describe phase and amplitude transients well enough to predict their effect onto a complex pulse-sequence numerically? To this end we have validated the model in different ways:

A) measurement with a small pickup coil positioned close to the sample coil

B) fitting of experimental curves with the presented model

C) numerical calculation of the coil current neglecting all nonlinear effects caused e.g. by diodes and amplifiers

A) The current in the sample coil is relatively big, hence it will induce a voltage into a small pick up coil [2] positioned nearby which serves as a measure of the coil current and can be detected with the help of an oscilloscope. Ideally pulse transients can be monitored experimentally with high time resolution with a pick up coil. However care has to be taken with respect to distortions which are caused by cables, mixers, filters and the oscilloscope itself used for the detection of the induced voltage. Significant distortions are already observed due to stray capacities if the pick up coil is placed close to the grounded outer probehead tube.

For this reason we have used an open probehead with removed outer tube, a 6-9 pF passive probe connected to a 500 MHz oscilloscope at $1\,\text{M}\Omega$ and a straight 6 cm copper

wire as antenna. We have tested the bandwidth of the RF generator of the NMR console and the bandwidth of the oscilloscope by feeding the low voltage signal directly into the oscilloscope. The observed pulse transients have a duration of approximately 50 ns. If the linear rf transistor amplifier and a 30 dB resistor are added, the transients do not become significantly longer. This setup results in a dataset of voltage versus time. The conversion from voltage-time to a dataset phase-amplitude-time is an under-determined problem. In order to obtain experimental values for current phase and amplitude versus time, we have chosen the dwell time of the oscilloscope for validation as $\frac{2\pi}{4\omega}$, so one experimental data point every 90° will be collected. Since phase and amplitude of the coil current change slowly in comparison with the time scale set by $\frac{2\pi}{\omega_{tr}}$, the data set can be converted to a series of phase and amplitude values sampled in steps of $\frac{2\pi}{4\omega_{tr}}$ using eqns. 8 and 9. Therein a single pair of phase and amplitude values at the time t is calculated from three experimental values of the real part of the current $Re\{\underline{a}_{total}(t)\}$ measured at t, $t - \frac{1}{4\omega}$ and $t + \frac{1}{4\omega}$.

$$\phi \cong \arctan\left(\frac{Re\{\underline{a}_{total}(t - \frac{1}{4\omega_{tr}})\} - Re\{\underline{a}_{total}(t + \frac{1}{4\omega_{tr}})\}}{2Re\{\underline{a}_{total}(t)\}}\right) - \omega_{tr}t \qquad (8)$$

$$A \cong \sqrt{Re\{\underline{a}_{total}(t)\}^2 + \left(\frac{Re\{\underline{a}_{total}(t - \frac{1}{4\omega_{tr}})\} - Re\{\underline{a}_{total}(t + \frac{1}{4\omega_{tr}})\}}{2}\right)^2} \qquad (9)$$

Since this data analysis averages over a time period of $\frac{1}{2\omega_{tr}}$, processing artifacts are to be expected when changes are no longer slow compared to the oscillation frequency ω_{tr}. In our experience artifacts can be neglected for changes slower than $\frac{1}{4\omega_{tr}}$.

Experimentally we have investigated the transient behavior with a windowless pulse train of 8 concatenated pulses

$(4\mu s)_{45°}-(4\mu s)_{225°}-(4\mu s)_{135°}-(4\mu s)_{315°}-(0.4\mu s)_{45°}-(0.4\mu s)_{135°}-(0.4\mu s)_{225°}-(0.4\mu s)_{315°}$

(notation: $(\text{pulse length})_{\text{phase}}$) for the following three cases, with the condition that the transmitter frequency and the frequency of the NMR transition are the same.

1. the probe was tuned and matched, so that the scattering-parameter spectrum $S_{11}(\omega)$ possesses a minimum at the transmitter frequency ω_{tr}.

2. as in 1. but minimum at $\omega_{tr}+0.41$ MHz

3. as in 1. but minimum at $\omega_{tr}+0.91$ MHz

Due to the increased detuning of the probe more power is being reflected by the probe. A pickup-coil was used to monitor the sample-coil current (Figure 1). Significant changes are observed depending on the amount of detuning which indicates that on a typical commercial spectrometer the generation of pulse transients is dominated by the probe-head and not by the rf generation and amplification. The transients have short time constants τ_R below $1\mu s$. Clearly, oscillations of phase and amplitude are present, which are predicted by the chosen simplified Mehring-Waugh model. Since the driving force of a transient is the factor $[A_m \exp(i\phi_m) - A_n \exp(i\phi_n)]$ in equation 3, it depends on the phase shift at the junction. Therefor the amplitude transients starting at the beginning of the second and fourth pulse look alike.

Transients may constructively or destructively interfere with the intended ideal pulse and may diminish the effective amplitude of a pulse. If strong pulses during a pulse sequence are needed to control interactions like the dipole-dipole coupling the strength of the rf field, i.e. its amplitude, should not fall below a certain value, because the

evolution of the spin dynamics would then be dominated by the internal interactions and not the pulse.

To observe a cumulative effect of transients, the pulse train finishes with four pulses of short duration compared to the circuit recovery time τ_R. Since the pulse phase of the four pulses has been chosen such that it is shifted by 90° to the phase of the pulse before, any deviation in the amplitude plot between the amplitude transients starting at time points 5, 6, 7 and 8 (Figure 1) can be ascribed to the cumulative effect of several transients as expressed in equation 7.

B) In order to validate the transient model (equation 3) the experimental transient curves were fitted with τ_R and ω_{eoff} as the only free parameters (see table 1). Corrections for linear changes in phase and amplitude were applied to the experimental data prior to fitting. We obtain good agreement between fitted and experimental curves (Figure 2), especially for small offset frequencies ω_{eoff}, which are typical for experimental conditions. Deviations can be explained by contributions of non-linear electronic elements in the oscilloscope, preamplifier or the power amplifiers. As previously shown [19] a probe deliberately mismatched and tuned off-resonance offers full control of the offset frequency ω_{eoff} . Consequently tuning offset and offset frequency correlate (see table 1).

When the rise-time τ_R is known, the frequency ω_{eoff} can be determined experimentally with a pulse-sequence of consecutive $(180_0 - 180_{180})_n$ -FID pulses. In a plot of signal amplitude versus n a sinusoidal modulation is observed. Its modulation frequency is a function of ω_{eoff}. If ω_{eoff} is zero, the frequency of the sinusoidal modulation is zero and no signal is observed. This sequence may also be used to find a suitable cable-length so that ω_{eoff} is zero.

C) The transient response of an arbitrary network of passive linear components can be simulated with programs like GNUCAP [28, 29]. For simulations we used a simplified circuit diagram of our double-resonance probe, taking into account only the X-channel (Figure 3) and assuming it is directly grounded on one side of the sample coil L_{sample}. The ^{1}H-frequency trap still remains in the X-branch. Fixed inductances and capacities can be estimated from the used hardware, while the matching inductance L_{match}, the tuning capacity C_{tune} and the resistance R were chosen such that the experimental spectrum of the scattering parameter is reproduced as good as possible by the numerically calculated one (diagram not shown).

For the calculation of the transient behavior we assumed a perfect voltage source at 50 Ohm impedance. Calculation for a pulse sequence of two short concatenated pulses allows to study the effect of pulse transients (Figure 4). We get almost perfect overlap between the fitted transient model (equation 3) and calculated curves even at big tuning offsets. The determined parameters τ_R and ω_{eoff} have similar values as the ones found in the experiments. For the probe tuned on-resonance at 83.333333 MHz the model parameters τ_R and $\frac{\omega_{eoff}}{2\pi}$ are $0.40\,\mu$s and -23 kHz, respectively, which have the same order of magnitude as the experimental values measured with a pick up coil on an open probe. We were able to verify [1] that a good estimate for τ_R is available from the probe band-width $\Delta \nu$ measured at the -3 dB line.

The second model parameter, the offset frequency ω_{eoff}, is found to be sensitive to cable-length effects in our setup. Cable-length effects are not expected in a system where the components amplifier, cables and duplexer have a characteristic impedance of exactly $50\,\Omega$. Numerical simulations indicate that in such an ideal system the parameter ω_{eoff} is much smaller than what we observe in our system. Therefor, we took into account other sources than only the probe-internal electronic circuits [3], namely

14

the impedance mismatch in the duplexer and the power amplifier. The impedance mismatch caused by imperfect coaxial cables was found to be negligible. Numerical simulations show how reflections which originate at a specific point of impedance mismatch cause quadrature transients which depend on the cable length l_{cable} between the point-of-impedance-mismatch to the probe (Figure 5): The ideal pulse P reaches the probe after passing though the cable. The probe initially will reflect part of the pulse because it has a finite rise-time τ_R. Therefor one part of the wave is consumed by the probe circuits and a second part R_1 is reflected. When R_1 propagates back through the cable it is partially reflected at the point-of-impedance-mismatch, which causes another pulse package R_2 traveling in the direction of the probe again. When R_2 has reached the probe it will have picked up a phase shift ϕ_{cable} of $2 \cdot l_{cable}/\lambda_{rf}$, where $\lambda_{rf} \approx \frac{2\pi \cdot c}{\omega_{tr}}$ is the wavelength of the radio-frequency pulse and c the speed of light. With the typical cable lengths found in a commercial spectrometer, all reflections and the original pulse are superimposed typically within less than $0.04 \mu s$ to form the sample coil current, which indicates that the simplified Mehring-Waugh model is still a good approximation of the transient behavior of the NMR pulses. If the reflections at the point-of-mismatch are bigger than the probe-internal quadrature transients [5], then a suitable cable length l_{cable} can be found so that the quadrature transients and ω_{eoff} become zero.

As expected, detuning the probe to $+0.41\,\text{MHz}$ and $+0.91\,\text{MHz}$ off the transmitter frequency affects the parameter $\frac{\omega_{eoff}}{2\pi}$ (table 1) which is shifted to higher values by 0.41 and $0.92\,\text{MHz}$, respectively. Note that ω_{eoff} can be controlled by the frequency to which the probe is tuned. In order to calculate arbitrary multiple-pulse sequences numerically exact we have implemented equation 7 as a Tcl script so it can be used with SIMPSON [30]. We conclude that the simplified model (equation 3) with two parameters τ_R and ω_{eoff} is sufficient to describe the calculated results even at moderate tuning or matching

15

offsets.

Table 1: Parameters τ_R and ω_{eoff} at a transmitter frequency of 83.333333 MHz obtained by fitting the response of a probe to a pulse sequence as shown in Figure 1.

$\omega_R - \omega_{tr}$ / MHz	$\tau_R/\mu s$	$\frac{\omega_{eoff}}{2\pi}$/kHz
0 (on resonance)	0.49	-172
+0.41	0.30	+607
+0.91	0.26	+1184

3   Transients And C-Based Pulse-Sequences

In general, a *robust* pulse sequence is thought to be insensitive towards unwanted interactions and insensitive towards pulse errors. Pulse transients are often considered as negligible, which –depending on the probe– may be true. However, during a cyclic pulse sequence even small pulse-non-idealities can lead to significant errors. As an example, we have chosen the popular pulse sequence PostC7 [12, 26] which –under the chosen conditions (vide infra)– should provide close to ideal suppression of the chemical shift interaction and very efficient double-quantum excitation [14]. All the presented results refer to ^{31}P double-quantum coherence generation under magic-angle-spinning on crystalline $Ag_7P_3S_{11}$ however similar experiments have been performed for ^{15}N, ^{13}C and ^{1}H (not shown).

3.1   PostC7 as an example for a C-symmetry sequence

PostC7 [26], alias $C7_2^1$ with a Post C-element, is a γ-encoded pulse sequence to convert zero-quantum (ZQ) to double-quantum (DQ) coherence, which allows a DQ filter with a theoretical efficiency of approx. 73% [8]. Non γ-encoded pulse sequences have only

16

50% theoretical efficiency [8]. Pulse sequences from the same family of CN_n^ν pulse sequences are able suppress the chemical shift interaction reliably to measure even small dipole-dipole couplings [12,14,26]. They consist of a pulse block used for two-spin DQ coherence excitation, followed by a pulse block to reconvert to zero-quantum coherence and they are terminated by a single read-pulse with 90° flip-angle after which the FID is detected (see Figure 6). Both DQ excitation and reconversion use the same rotor-synchronized multiple-pulse sequence from the C-symmetry library [8], whose appearance is determined by the three symmetry numbers $N = 7$, $n = 2$, $\nu = 1$ (for $C7_2^1$), the C-element $C = 90_0 - 360_{180} - 270_0$ (the "Post" C-element, notation: $flip\,angle_{phase}$) and a supercycle which repeats the C-cycle with all phases shifted by 180° [31], which is also called π-shifted cycle [32]. The duration of excitation $\tau_{DQ,exc}$ and reconversion $\tau_{DQ,recon}$ can be controlled by repeating the PostC7 sequence several times. Similar sequences from the C-symmetry library use the same C-element and supercycle, but different symmetry numbers N, n and ν. A cogwheel Cog12(2,5,6;0) phase cycle [14,33] is used to select the coherence order pathways $p = \{0 \to 2 \to 0 \to -1; 0 \to -2 \to 0 \to -1\}$.

It has been noted before [14] that pulse transients influence the DQ filtered intensity E_{DQ} (defined as DQ filtered peak area over peak area of a direct excitation spectrum under similar conditions) of PostC7, which becomes evident from a plot of E_{DQ} as a function of the nutation frequency ν_{rf} (=radio frequency amplitude, defined as the inverse of the length of a pulse with 360° flip angle). Consequently, also DQ build-up curves deviate from the expected ideal behavior. Long conversion periods are necessary to determine weak couplings, which makes the experiment sensitive to small pulse errors. As can be seen in Figure 8 pulse transients seriously reduce the conversion efficiency and even may cause negative values for build-up curves which have been acquired with a symmetric protocol ($\tau_{DQ,exc} = \tau_{DQ,recon}$) [14]. Neither of these effects is

desired. Because the numerically exact spin-dynamics simulation (Figure 8) took into account only the homonuclear through-space dipole-dipole interaction, we conclude, that the chemical shift is not necessary for pulse transients to spoil the performance of PostC7.

How will pulse transients influence the PostC7 sequence? C-sequences are built on the premises that the pulses form a cycle. The magnetization of a single spin-1/2 which is subject to a PostC7 sequence should therefor move on a trajectory [34] which repeats after each full C-cycle (see Figure 7). This is no longer true when pulse transients are considered. The effective pulse field at the sample no longer consists of piecewise defined functions of constant pulse phase and amplitude but consists rather of continuous functions which have a non-trivial influence on the single-spin magnetization trajectory. Numerical simulations indicate that the C-cycle looses its cyclicity when pulse transients are active which causes the observed degradation of the pulse-sequence (see Figure 6).

Quadrature transients are under the control of the spectrometer operator. With the help of the above mentioned pulse sequence $(180_0 - 180_{180})_n$ -*FID* and a line-stretcher we adjusted the cable length l_{cable} to make the quadrature transients vanish ($\omega_{eoff} = 0$). The DQ excitation curve improve a little bit but still significant deviations from the expected response are observed (Figure not shown). We conclude that pulse transients may cause high losses in simple DQ experiments.

3.2 γ-Encoded Transient Adapted C-Sequences

In the following we describe how γ-encoded C-sequences can be modified to significantly reduce the effect of pulse transients. The simple idea is to use a modified C-

element which tries to compensate the pulse transients in the sense that a single-spin polarization vector in a Bloch picture performs rotations close to an ideal trajectory without pulse transients. A consequence of this approach is that experiments done with the transient adapted C-sequences can be analyzed as usual. For this purpose the Post-C element is replaced by a "phase-tuned" element, $C = 90_\zeta - 360_{180} - 270_0$, whose phase ζ is optimized once for a given setup. It shares some similarities with the "phase-tuned" R-element which has been proposed by Carravetta et al. [13] in order to compensate for chemical shift effects. In our case ζ typically takes optimal values between $-3°$ and $+3°$. Optimization is achieved by finding the values of ζ for which the intensity of the DQ filtered signal is maximum. A plot of the DQ-filtered intensity against phase ζ ("phase-tuning-plot") is displayed in Figure 9. The same shape is observed for all experiments we have performed (^{1}H , ^{15}N, ^{13}C, ^{31}P), also in higher magnetic fields like ^{13}C$_2$-glycine in a magnetic field of 11.74 T (see supporting information, Fig. S1 and S2) and also for a numerical simulation on the basis of the transient formula described above. Simulations with varying offset frequency ω_{eoff} indicate that ω_{eoff} causes a significant shift of the optimum phase ζ and also a small change in conversion efficiency. For this reason it is a good idea to minimize ω_{eoff} by cable-length effects as described above. With the described phase-tuned C-element we have been able to improve the DQ filtered intensity in some cases from 0% to reasonable values (^{15}N NMR of NH$_4$Cl), in cases of ^{31}P-NMR we often find twice the amount of signal intensity after optimization depending on the rise time of the probe. On the other hand, ^{1}H NMR experiments performed on the same probe, however on a separate channel dedicated to the ^{1}H frequency, hardly show any influence of quadrature pulse transients, possibly because it is easier to match impedance over the complete line of used hardware (amplifier - preamplifier - probe) than for an "X" channel experiment which has to cover

19

a wider frequency range. Consequently fewer reflections contribute to the generation of quadrature transients. Moreover we have experimentally verified that the approach also works for other double-quantum sequences from the C-symmetry library (e.g. $C7_1^3$, $C9_1^4$, $C11_1^5$...) [35]. It should be noted that the sensitivity of γ-encoded C-sequences towards pulse-transients increases the longer the conversion times τ_{DQ} and the higher the necessary radio-frequency amplitudes ν_{rf} are. Therefor transient-adapted PostC7 shows a sharper maximum in the phase-tuning plot at 20 kHz than at 10 kHz (Figure 9) sample spinning frequency.

The impact of a phase-tuned C-element is visualized with the help of single-spin polarization trajectories (Figure 7). The phase-tuned C-element restores the cyclicity of the full C-cycles, so that the trajectories of several consecutive C-cycles exactly overlap and the relevant single-spin interaction, the chemical shift, is suppressed. We note that the simulated and the experimental phase-tuning plot are in reasonable agreement which indicates that the design of pulse-transient compensated pulse sequences on the basis of the above-mentioned formulas is possible in general. Simulations indicate that the 180°-supercycle on a full C-cycle reduces the influence on transients, but the supercycle is not able to compensate pulse-transients as the phase-tuned C-element is.

4 Experimental Section

NMR: The ^{31}P NMR experiments were carried out on a Bruker Avance-II NMR spectrometer equipped with a commercial 2.5 mm double-resonance (H/X) MAS-NMR probe. The magnetic field strength was 4.7 T corresponding to a resonance frequency of $\nu\left(^{31}\text{P}\right) = 81.1$ MHz. Samples were rotated within zirconia spinners. A commercially available pneumatic control unit was used to limit MAS frequency variations to a

2 Hz interval for the duration of the experiment. For crystalline $Ag_7P_3S_{11}$ the spinning frequency ν_{MAS} was set to 10 kHz when not mentioned otherwise. During the PostC7 sequence this required pulse nutation frequencies ν_{rf} of 70 kHz. A saturation comb was used to erase the phase memory of the spins, since the used repetition delays of $10 - 32$ s were too short with respect to spin-lattice relaxation times. The saturation comb was used in front of every scan and typically consisted of 10-20 pulses with a 90° flip-angle and a delay of 50 ms. Radiofrequency pulses were generated on an SGU600 board of the Avance-II console and amplified through a Bruker BLAX500 transistor amplifier ($6 - 365$ MHz bandwidth, class AB). The reflections at the output of the power amplifier proved to be important for controlling the quadrature component of the pulse transients.

The numerical simulations of the spin-dynamics were done using the SIMPSON NMR interpreter by Nielsen and co-workers [30, 36]. Powder averages were chosen according to the Zaremba-Conroy-Wolfsberg scheme [37] with a number of 1760 orientations (88 α-, β-angle-pairs times 20 γ-angles) or better, to achieve convergence of the powder average. The integration time step for the DQ simulations was chosen as 1/357th of the shortest rf-unit in the pulse sequence, i.e. 10 ns or smaller. Numerically exact pulse transient simulations were performed with a procedure implementing the formula described eq.(7) with the program SIMPSON in the scripting language Tcl (compatible with version 8.4 and 8.5). The transient procedure allows the calculation of cyclically used pulse blocks and used a cut-off delay of 6 μs, which is the longest period up to which a discontinuity was assumed to have an influence on pulse amplitude and pulse phase after its occurrence.

Electronics: The parameters for the equivalent circuit diagram in Figure 3 were chosen as follows: $C_{tune} = 22.11$ pF, $L_{match} = 8.95$ nH, $C_{trap} = 18.2$ pF, $L_{trap} = 34.8$ nH,

$L_{sample} = 114\,\text{nH}$, $R = 0.435\,\Omega$. The resistance R was determined by adjusting R until an experimental scattering parameter spectrum $S_{11}(\omega)$ of the probe measured on a network analyzer is reproduced by simulation. The band width was determined from the -3 dB line in $S_{11}(\omega)$-spectrum [2]. Coarse cable length adjustments were realized with self-assembled coaxial-cables using identical type-N connectors which were crimped onto RG214 cables of variable length. Fine adjustments were implemented with the help of a trombone-type line-stretcher (Microlab/FXR ST-05N) at almost constant impedance of $50\,\Omega$.

The sample coil currents were monitored through mutual-inductive coupling a small pickup coil (approx. 6 cm copper wire) connected with a passive probe (HP 1160A) connected to a digital oscilloscope (Hewlett Packard Infinium 54280A oscilloscope, 500 MHz, 2 GSa/s).

Simulations of scattering parameter spectra were achieved with the program ViPEC [38]. Calculations of transients were executed with the program GNUCAP [29, version 0.35]. Scattering parameter measurements were performed with an Agilent 8712ES RF vector network analyzer.

5   Conclusions

In this contribution we have shown that C-symmetry based pulse sequences used for double-quantum filtering experiments under typical experimental conditions are influenced by pulse amplitude and phase transients. Based on a simple model for the description of pulse transients we were able to develop a phase-tuned C-element which can be applied to γ-encoded C-sequences to reconstitute an almost theoretical performance. The chosen rather simple approach shows a tremendous increase in the exper-

imentally observed double-quantum efficiencies which may make it useful for double-quantum filtered experiments where C-sequences have their domain, i. e. small dipole-dipole couplings and big shielding tensors. Especially for small sample rotor diameters ($\leq 2.5\,\text{mm}$) and low Larmor frequencies we have found that not the pulse power but the pulse transients were the bottle neck for the performance of the pulse sequences which can be overcome with phase-adapted supercycled C-sequences.

6 Acknowledgments

7 Supporting Information Available

Phase adapted PostC7 applied to $^{13}C_2$-glycine at a sample spinning frequency of 20 kHz and at a magnetic field of 11.74 T.

References

[1] J. D. Ellett, M. G. Gibby, U. Haeberlen, L. M. Huber, M. Mehring, A. Pines, and J. S. Waugh, Spectrometers for multiple-pulse NMR, *Adv. Magn. Reson.* **5**, 117–176 (1971).

[2] J. Mispelter, M. Lupu, and A. Briguet, *NMR probeheads for biophysical and biomedical experiments: theoretical principles & practical guidelines*, Imperial College Press, London (2006).

[3] R. Prigl and U. Haeberlen, The theoretical and practical limits of resolution in multiple-pulse high-resolution NMR of solids, *Adv. Magn. Opt. Reson.* **19**, 1–58 (1996).

[4] D. I. Hoult and R. E. Richards, The signal-to-noise ratio of the nuclear magnetic resonance experiment, *J. Magn. Reson.* **24**, 71–85 (1976).

[5] M. Mehring and J. S. Waugh, Phase transients in pulsed NMR spectrometers, *Rev. Sci. Instrum.* **43**, 649–653 (1972).

[6] C. T. Kehlet, A. C. Sivertsen, M. Bjerring, T. O. Reiss, N. Khaneja, S. J. Glaser, and N. C. Nielsen, Improving solid-state NMR dipolar recoupling by optimal control, *J. Am. Chem. Soc.* **126**, 10202–10203 (2004).

[7] D. Iuga, H. Schäfer, R. Verhagen, and A. P. M. Kentgens, Population and coherence transfer induced by double frequency sweeps in half-integer quadrupolar spin systems, *J. Magn. Reson.* **147**, 192–209 (2000).

[8] M. H. Levitt, Symmetry-based pulse sequence in magic-angle spinning solid-state NMR, *Encyc. NMR* **9**, 165–196 (2002).

[9] M. Feike, D. E. Demco, R. Graf, J. Gottwald, S. Hafner, and H. W. Spiess, Broadband multiple-quantum NMR spectroscopy, *J. Magn. Reson.* **A122**, 214–221 (1996).

[10] L. Bosman, P. Madhu, S. Vega, and E. Vinogradov, Improvement of homonuclear dipolar decoupling sequences in solid-state nuclear magnetic resonance utilising radiofrequency imperfections, *J. Magn. Reson.* **169**, 39–48 (2004).

[11] M. Leskes, P. K. Madhu, and S. Vega, Proton line narrowing in solid-state nuclear magnetic resonance: New insights from windowed phase-modulated Lee-Goldburg sequence, *J. Chem. Phys.* **125**, 124506 (2006).

[12] Y. K. Lee, N. D. Kurur, M. Helmle, O. G. Johannessen, N. C. Nielsen, and M. H. Levitt, Efficient dipolar recoupling in the NMR of rotating solids. A sevenfold symmetric radiofrequency pulse sequence, *Chem. Phys. Lett.* **242**, 304–309 (1995).

[13] M. Carravetta, M. Edén, O. G. Johannessen, H. Luthman, P. J. E. Verdegem, J. Lugtenburg, A. Sebald, and M. H. Levitt, Estimation of carbon-carbon bond lengths and medium-range internuclear: Distances by solid-state nuclear magnetic resonance, *J. Am. Chem. Soc.* **123**, 10628–10638 (2001).

[14] J. Schmedt auf der Günne, Distance measurements in spin-1/2 systems by ^{13}C and ^{31}P solid-state NMR in dense dipolar networks, *J. Magn. Reson.* **165**, 18–32 (2003).

[15] J. Schmedt auf der Günne, Effective dipolar couplings determined by dipolar dephasing of double-quantum coherences, *J. Magn. Reson.* **180**, 186–196 (2006).

[16] T. Frey and M. Bossert, *Signal- und Systemtheorie*, Teubner, Stuttgart; Leipzig; Wiesbaden, 1 edition (2004).

[17] Y. Tabuchi, M. Negoro, K. Takeda, and M. Kitagawa, Total compensation of pulse transients inside a resonator, *J. Magn. Reson.* **204**, 327–332 (2010).

[18] A. J. Vega, Controlling the effects of pulse transients and RF inhomogeneity in phase-modulated multiple-pulse sequences for homonuclear decoupling in solid-state proton NMR, *J. Magn. Reson.* **170**, 22–41 (2004).

[19] G. C. Chingas, Overcoupling NMR probes to improve transient response, *J. Magn. Reson.* **54**, 153–157 (1983).

[20] D. P. Burum, M. Linder, and R. R. Ernst, A new "tune-up" NMR pulse cycle for minimizing and characterizing phase transients, *J. Magn. Reson.* **43**, 463–471 (1981).

[21] W. K. Rhim, D. D. Elleman, L. B. Schreiber, and R. W. Vaughan, Analysis of multiple pulse NMR in solids. II, *J. Chem. Phys.* **60**, 4595–4604 (1974).

[22] R. W. Vaughan, D. D. Elleman, L. M. Stacey, W. K. Rhim, and J. W. Lee, A simple, low power, multiple pulse NMR spectrometer, *Rev. Sci. Instrum.* **43**, 1356 (1972).

[23] J. J. Spokas, Means of reducing ringing times in pulsed nuclear magnetic resonance, *Rev. Sci. Instrum.* **36**, 1436 (1965).

[24] K. E. Kisman and R. L. Armstrong, Coupling scheme and probe damper for pulsed nuclear magnetic resonance single coil probe, *Rev. Sci. Instrum.* **45**, 1159 (1974).

[25] A. S. Peshkovsky, J. Forguez, L. Cerioni, and D. Pusiol, RF probe recovery time reduction with a novel active ringing suppression circuit, *J. Magn. Reson.* **177**, 67–73 (2005).

[26] M. Hohwy, H. J. Jakobsen, M. Edén, M. H. Levitt, and N. C. Nielsen, Broadband dipolar recoupling in the nuclear magnetic resonance of rotating solids: A compensated C7 pulse sequence, *J. Chem. Phys.* **108**, 2686–2694 (1998).

[27] H. H. Meinke and F. Gundlach, *Taschenbuch der Hochfrequenztechnik I: Grundlagen*, Springer, Berlin, 5 edition (2009).

[28] T. M. Barbara, J. F. Martin, and J. G. Wurl, Phase transients in NMR probe circuits, *J. Magn. Reson.* **93**, 497–508 (1991).

[29] A. T. Davis, An overview of algorithms in gnucap, *IEEE University/Government/Industry Microelectronics Symposium, 2003. Proceedings of the 15th Biennial* 360–361 (2003).

[30] M. Bak, J. T. Rasmussen, and N. C. Nielsen, SIMPSON: A general simulation program for solid-state NMR spectroscopy, *J. Magn. Reson.* **147**, 296–330 (2000).

[31] M. Hohwy, C. M. Rienstra, C. P. Jaroniec, and R. G. Griffin, Fivefold symmetric homonuclear dipolar recoupling in rotating solids: Application to double quantum spectroscopy, *J. Chem. Phys.* **110**, 7983–7992 (1999).

[32] P. E. Kristiansen, M. Carravetta, W. C. Lai, and M. H. Levitt, A robust pulse sequence for the determination of small homonuclear dipolar couplings in magic-angle spinning NMR, *Chem. Phys. Lett.* **390**, 1–7 (2004).

[33] M. H. Levitt, P. K. Madhu, and C. E. Hughes, Cogwheel phase cycling, *J. Magn. Reson.* **155**, 300–306 (2002).

[34] M. H. Levitt, *Spin Dynamics: Basics of Nuclear Magnetic Resonance*, Wiley (2001).

[35] A. Brinkmann, M. Edén, and M. H. Levitt, Synchronous helical pulse sequences in magic-angle spinning nuclear magnetic resonance: Double quantum recoupling of multiple-spin systems, *Journal of Chemical Physics* **112**, 8539–8554 (2000).

[36] T. Vosegaard, A. Malmendal, and N. C. Nielsen, The flexibility of SIMPSON and SIMMOL for numerical simulations in solid- and liquid-state NMR spectroscopy, *Monatsh. Chem.* **133**, 1555–1574 (2002).

[37] H. Conroy, Molecular Schrödinger equation. VIII. A new method for the evaluation of multidimensional integrals, *J. Chem. Phys.* **47**, 5307–5318 (1967).

[38] J. Rossouw and A. Jansen, http://vipec.sourceforge.net/, *version 3.2.0* (2003).
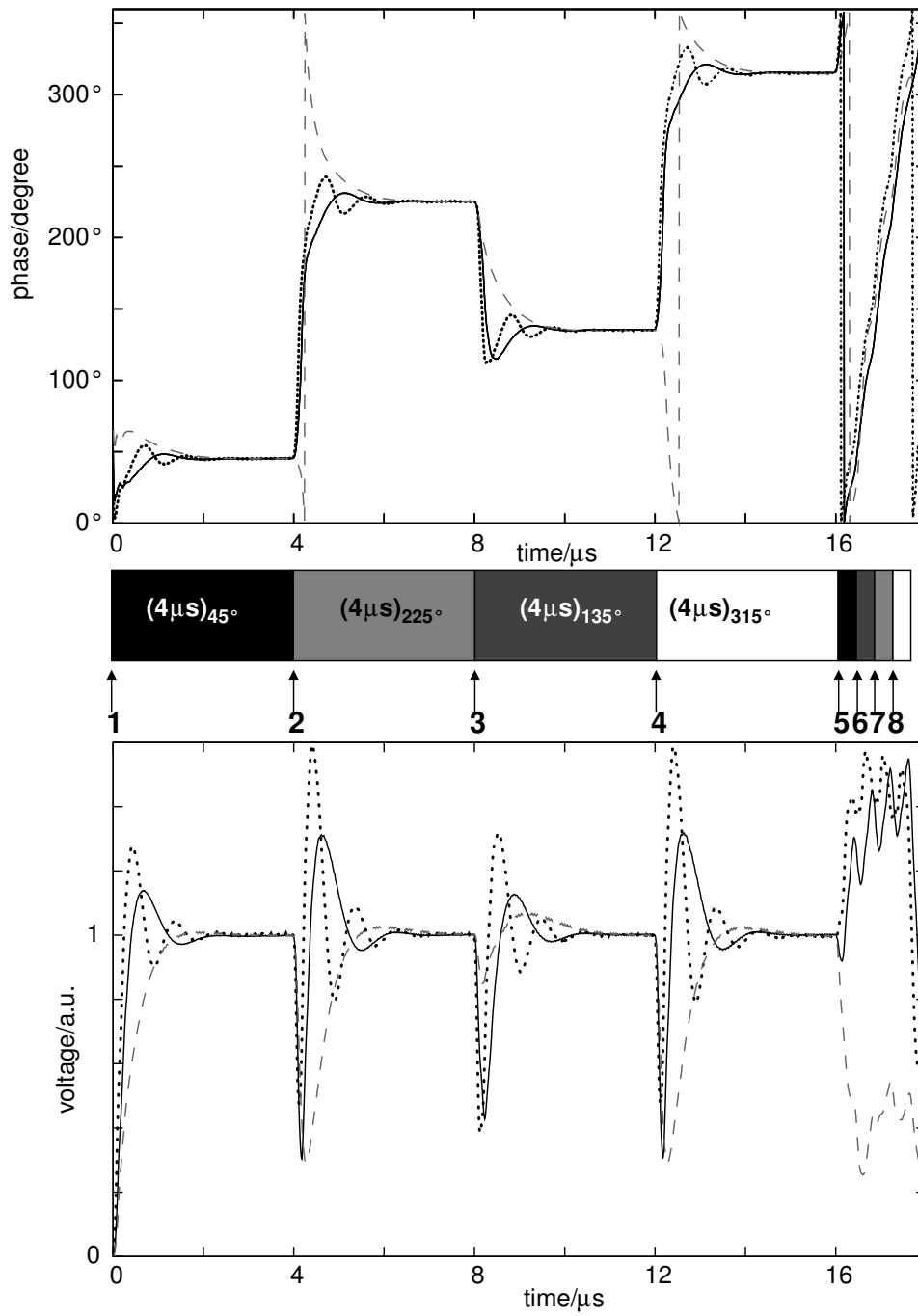
Figure 1: Phase and amplitude transients of a windowless eight-pulse sequence measured with a pickup coil close to the sample-coil of a probehead (see text for details); dashed lines refer to a probe tuned to the minimum of the scattering parameter spectrum $S_{11}(\omega)$; solid and dotted lines refer to a the probe tuned and matched with an offset of 0.41 MHz and 0.91 MHz, respectively.

29
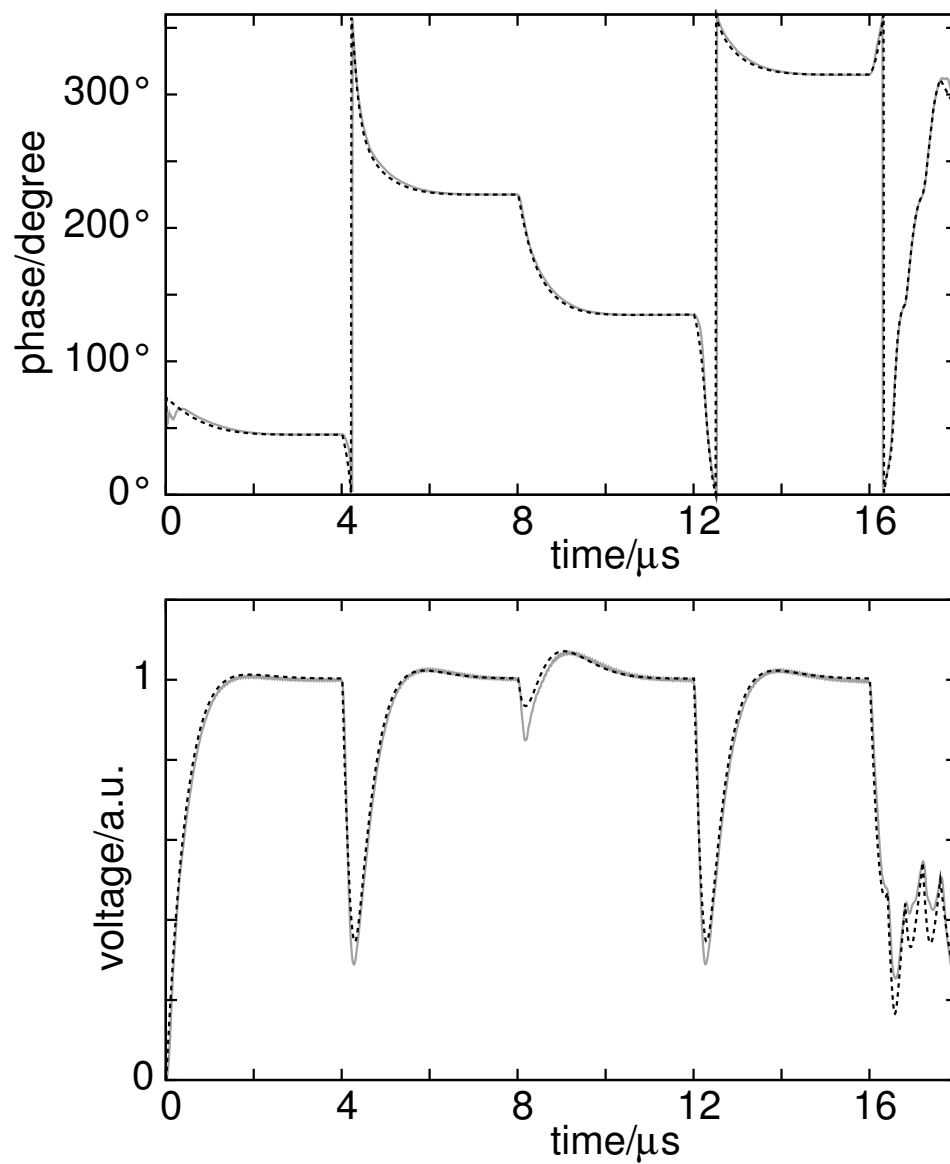
Figure 2: Phase and amplitude transients of a windowless eight-pulse sequence measured with a pickup coil close to the sample-coil of a open probehead (grey solid line, see text) of a probe tuned on the magnitude of the scattering parameter; the dashed line shows the best fit using equations 7, 8 and 9.
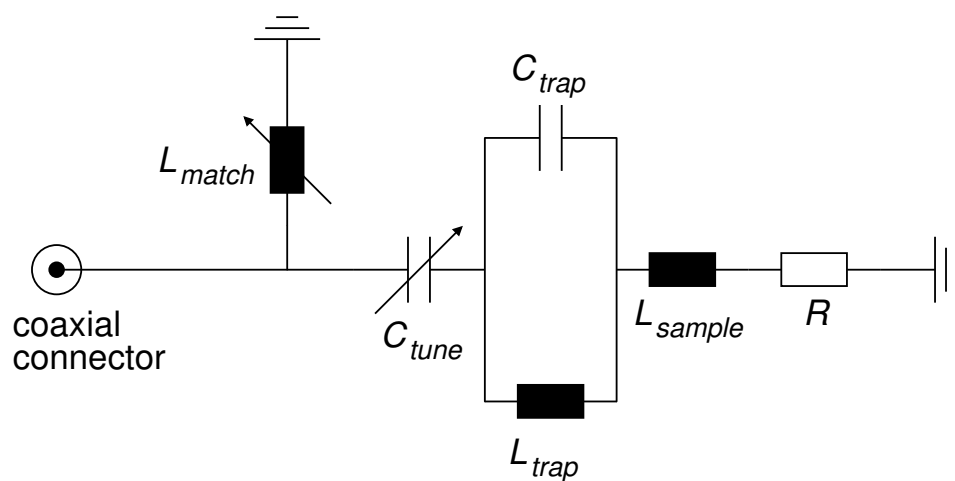
Figure 3: Simplified equivalent circuit diagram for the X-channel branch of the used double-resonance NMR probe, which was used for transient calculations.
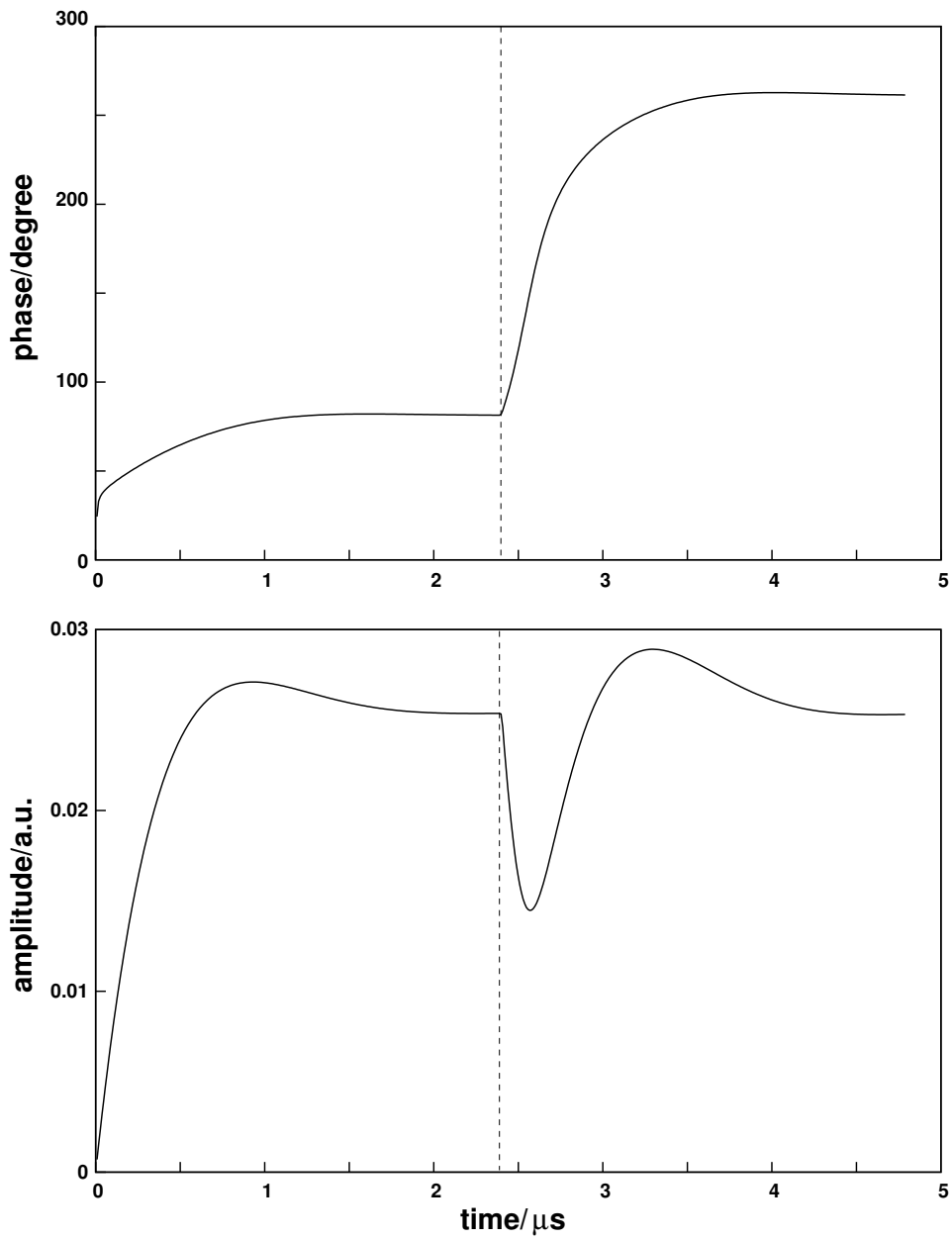
Figure 4: Calculated pulse transients from the electric response of the circuit described in Figure 3 to a two-pulse sequence with 2.4 μs length and shifted by 180°; upper graph: phase, lower graph: amplitude.
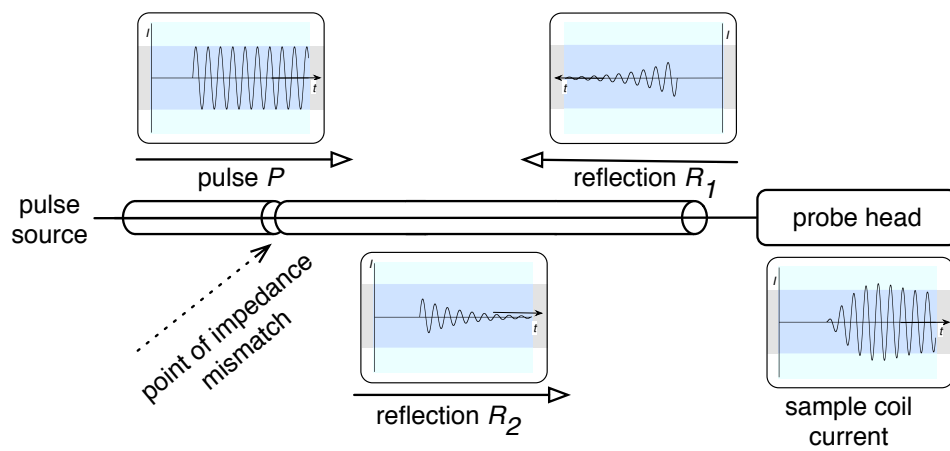
Figure 5: Reflections illustrated for a simplified circuit including a probehead.
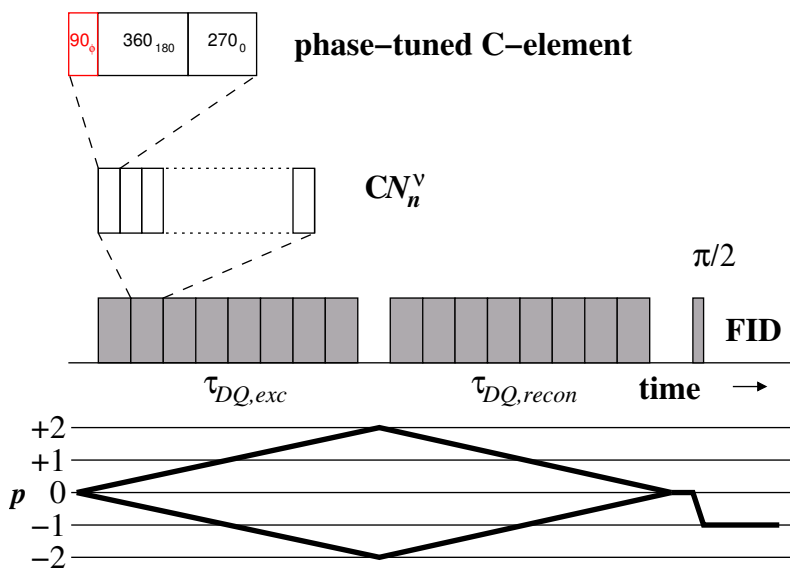
Figure 6: Scheme of a transient-adapted CN_n^ν sequence with a phase tunable C-element; the coherence transfer pathway indicates which coherence orders p are selected by the phase cycling scheme;
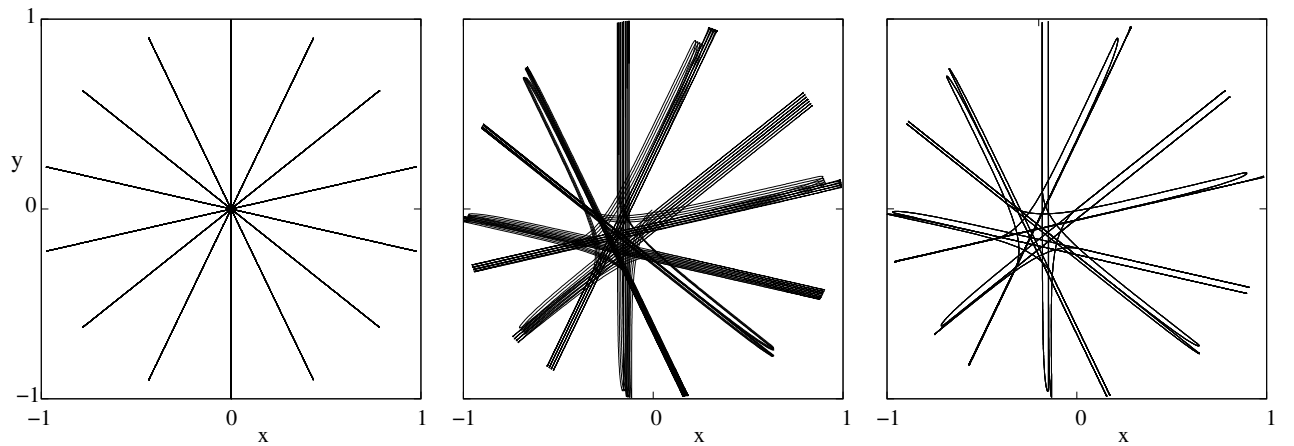
Figure 7: Projections of simulated single-spin magnetization trajectories onto the XY-plane of the rotating frame during a PostC7 sequence for an evolution upto three complete non-supercycled C-cycles; ideal (left), including pulse transients (middle), including pulse transient but using transient-adapted PostC7 (right); the simulations were performed for a 2-spin system with a dipole coupling ν_{dip} of $-436\,$Hz, an τ_R of $0.49\,\mu$s and an $\omega_{eoff}/(2\pi)$ of $-68.7\,$kHz; the phase ζ in phase-adapted PostC7 was $0.4793°$; note that the 2nd and 3rd cycle for phase-adapted PostC7 overlap with the first cycle, while the trajectories for ordinary PostC7 sequence fan out.
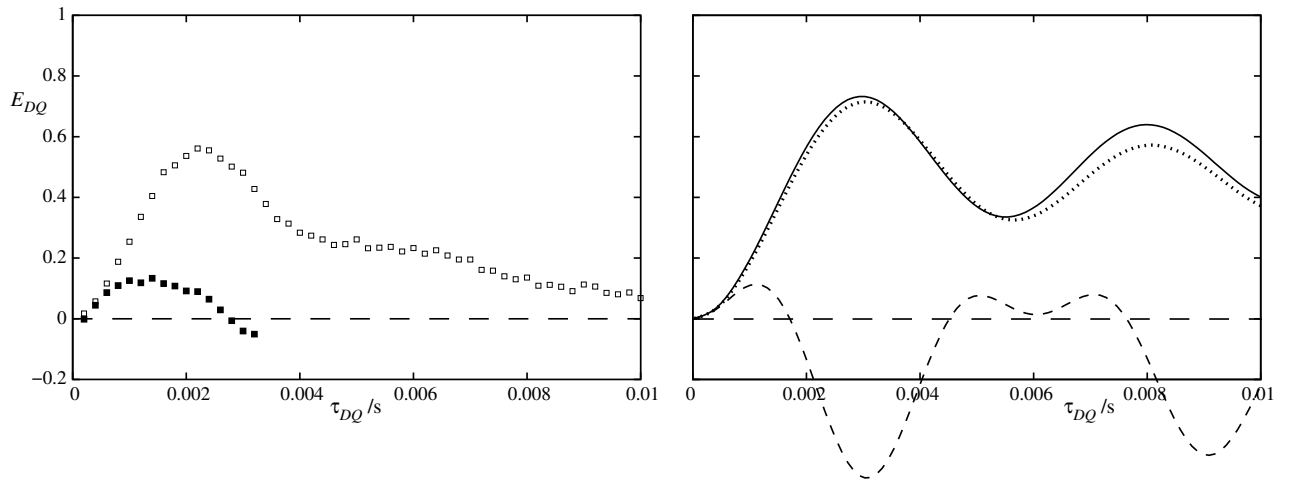
Figure 8: Double-quantum filtered intensity E_{DQ} for a supercycled PostC7 sequence as a function of the conversion time τ_{DQ}; simulations (right): ideal behavior from a numerical simulation without pulse transients (solid black line), including pulse transients (dashed curve), including pulse transient but using transient-adapted PostC7 (dotted curve); experiment (left): obtained by PostC7 (filled squares), obtained by transient-adapted PostC7 (open squares); almost perfect agreement between simulated and experimental curve of transient-adapted PostC7 can be obtained by including a monoexponential damping factor for the simulations (not shown).
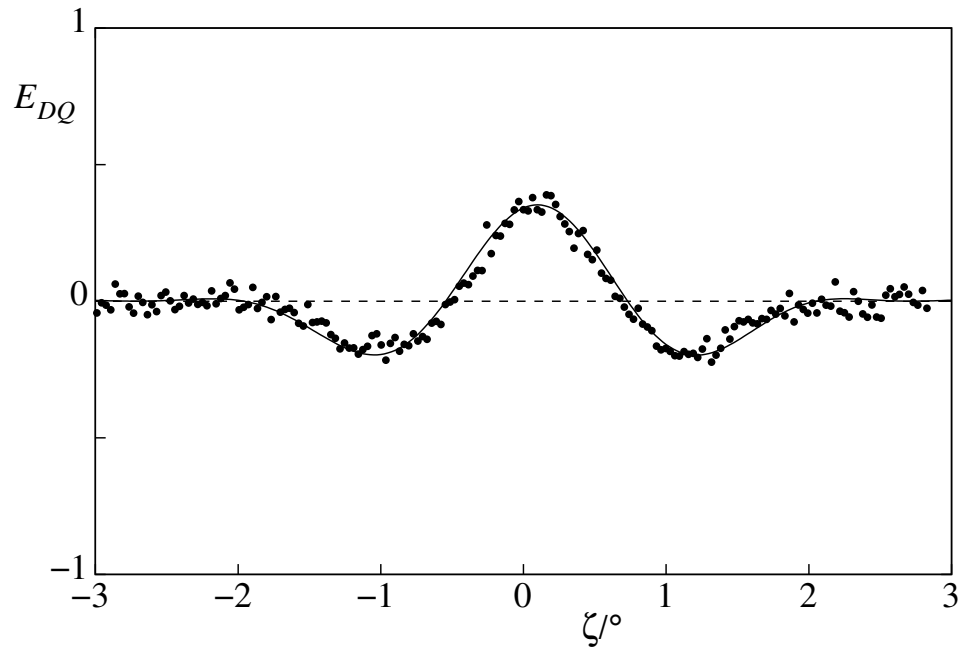
Figure 9: Double-quantum filtered intensity E_{DQ} for a phase-adapted supercycled PostC7 experiment as a function of the phase ζ ("phase-tuning plot") with a constant conversion time τ_{DQ} of 2 ms; experimental values (filled circles) versus simulated curves (solid line) at a sample spinning frequency of $\nu_r = 10$ kHz; the simulation was performed for a 2-spin system with a dipole coupling ν_{dip} of -436 Hz and τ_R of $0.49\,\mu$s; the offset frequency ω_{eoff} and the scaling factor for E_{DQ} were adjusted to obtain an overlap with the experiment data points.